The first high-redshift Changing Look Quasars

Nicholas P. Ross[1]★, Matthew Graham[2], K. E. Saavik Ford[3,4,5], Barry McKernan[3,4,5]
Daniel Stern[6] and Giorgio Calderone[7]
[1]Institute for Astronomy, University of Edinburgh, Royal Observatory, Blackford Hill, Edinburgh EH9 3HJ, United Kingdom
[2]Cahill Center for Astronomy and Astrophysics, California Institute of Technology, Mail Code 249/17, 1200 E California Blvd, Pasadena CA 91125, USA
[3]Department of Science, BMCC, City University of New York, New York, NY 10007, USA
[4]Department of Astrophysics, Rose Center for Earth and Space, American Museum of Natural History, Central Park West at 79th Street, NY 10024, USA
[5]Graduate Center, City University of New York, 365 5th Avenue, New York, NY 10016, USA
[6]Jet Propulsion Laboratory, California Institute of Technology, 4800 Oak Grove Drive, Mail Stop 169-221, Pasadena, CA 91109, USA
[7]INAF – Osservatorio Astronomico di Trieste, Via Tiepolo 11, I-34143 Trieste, Italy

Accepted XXX. Received YYY; in original form ZZZ

ABSTRACT

We report on three redshift $z > 2$ quasars with dramatic changes in their C IV emission lines, the first "Changing-Look" quasars at high redshift. This is also the first time the changing-look behaviour has been seen in a high-ionization emission line. SDSS J1205+3422, J1638+2827 and J2228+2201 show interesting behaviour in their observed optical light curves, and subsequent spectroscopy shows significant changes in the C IV broad emission line, with both line collapse and emergence being displayed in rest-frame timescales of ∼240-1640 days. These are very quick changes, especially when considering virial black hole mass estimates have all three quasars with $M_{\rm BH} > 10^9 M_\odot$. Continuum and emission line measurements from the three quasars show changes in the continuum-equivalent width plane with the CLQs seen to be on the edge of the full population distribution, and showing indications of an intrinsic Baldwin Effect. We put these observations in context with recent "state-change" models, but note that even in their 'low-state', the C IV CLQs are above ∼10% in Eddington luminosity.

Key words: accretion, accretion discs – surveys – quasars: general – quasars: time-domain:

1 INTRODUCTION

Luminous AGN, i.e. quasars, are now seen to significantly vary their energy output on timescales as short as weeks to months. This observation, and the subsequent mismatch in the expected "viscous" timescale, which for a 10^7 M$_\odot$ central supermassive black hole (SMBH) is ∼hundreds of years, was noted over 30 years ago (e.g. Alloin et al. 1985). However, with new photometric light-curve and repeat spectroscopic data, the desire for a deeper understanding of AGN accretion disk physics has recently re-invigorated the field (e.g. Antonucci 2018; Lawrence 2018; Ross et al. 2018; Stern et al. 2018).

The optical continuum variability of quasars has been recognized since their first optical identification (e.g., Matthews & Sandage 1963; MacLeod et al. 2012). Dramatic changes in the broad emission lines (BELs) of quasars has only recently been identified (e.g., LaMassa et al. 2015). Samples of over 100 "Changing Look" quasars (CLQs) or "Changing State" quasars (CSQs) have now been assembled (e.g. MacLeod et al. 2019; Graham et al. 2019a). The community uses both these terms as a cover for the underlying physics. For sake of argument, CLQs can potentially be thought of as the extension to the BELs of quasar continuum variability (e.g., MacLeod et al. 2012) whereas the CSQs have a 'state-transition' similar to that in Galactic X-ray binaries (Noda & Done 2018; Ruan et al. 2019). In this paper, we use the term 'Changing Look', as we are currently agnostic, and confessedly ignorant, to the underlying physical processes.

CLQs to date have primarily been defined according to the (recombination) Balmer emission line properties with particular attention paid to the Hβ emission line, observed from optical spectroscopy. Recent work report on discoveries of Mg II Changing-look AGN (Guo et al. 2019; Homan et al. 2019). However, current CLQ studies have primarily been at redshifts $z < 1$.

While there have been many studies on triply ionized carbon, i.e C IV, these have tended to focus on broad absorption line quasars (BAL quasars; see Table 1 of Hemler et al. 2019) or the Baldwin Effect (BEff; Baldwin 1977; Bian et al. 2012; Jensen et al. 2016; Hamann et al. 2017)[1]. Dramatic changes in the collisionally excited

[1] As noted in Rakić et al. (2017), two different types of Baldwin effect are present in the literature: the *global* (or *ensemble*) Baldwin Effect, which is an anti-correlation between the Equivalent Width (EW) of the emission line and the underlying continuum luminosity of *single-epoch* observations

★ E-mail: npross@roe.ac.uk

Line	λ / Å	Transition energy / eV	Ionization energy / eV	Transition Levels Lower			Upper			Wavenumber / cm^{-1}	$A_{i,j}$ ($\times 10^8$ / s^{-1})
H LyLim	912.324	13.5984	13.5984	$1s$	^{2}S	1/2	∞			109 678.7	1.23$\times 10^{-6}$
H Lyα	1215.670	10.1988	13.5984	$1s$	^{2}S	1/2	2			82 259.2	4.67
N v	1238.821	10.0082	97.8901	$1s^22s$	^{2}S	1/2	$1s^22p$	^{2}P^o	3/2	80 721.9	3.40
N v	1242.804	9.9762	97.8901	$1s^22s$	^{2}S	1/2	$1s^22p$	^{2}P^o	1/2	80 463.2	3.37
C iv	1548.187	8.0083	64.4935	$1s^22s$	^{2}S	1/2	$1s^22p$	^{2}P^o	3/2	64 591.7	2.65
C iv	1550.772	7.9950	64.4935	$1s^22s$	^{2}S	1/2	$1s^22p$	^{2}P^o	1/2	64 484.0	2.64
[He ii]	1640.474	7.5578	54.4178	$2p$	^{2}P^o	3/2	$3d$	^{2}D	5/2	60 958.0	10.35
[He ii]	1640.490	7.5578	54.4178	$2p$	^{2}P^o	3/2	$3d$	^{2}D	3/2	60 957.4	1.73
C iii]	1906.683	6.5026	47.8878	$1s^22s^2$	^{1}S	0	$1s^22s2p$	^{3}P^o	2	52 447.1	5.19$\times 10^{-11}$
C iii]	1908.734	6.4956	47.8878	$1s^22s^2$	^{1}S	0	$1s^22s2p$	^{3}P^o	1	52 390.8	1.14$\times 10^{-6}$
Mg ii	2795.528	4.4338	15.0353	$2p^63s$	^{2}S	1/2	$2p^63p$	^{2}P^o	3/2	35 760.9	2.60
Mg ii	2802.705	4.4224	15.0353	$2p^63s$	^{2}S	1/2	$2p^63p$	^{2}P^o	1/2	35 669.3	2.57
H Ba β	4861.333	2.5497	13.5984	2			4			20 564.8	0.0842

Table 1. Strong UV/optical spectral emission lines in quasars, and their atomic data. Data from the NIST Atomic Spectra Database (Kramida et al. 2018; Kramida et al. 2019). The Transition Energies are $E = hc/\lambda$ for the given wavelength. The Ionization Energy is the energy required to ionize the given species, e.g. 64.49 eV are needed to create a C v ion. Transitions Level configurations are given in standard spectroscopic notation $A_{i,j}$ are transition probabilities. Data from the NIST Atomic Spectra Database (Kramida et al. 2018; Kramida et al. 2019).

broad *emission* line (BEL) of C iv and indeed C iii] have not to this point been reported.

Here, we present new results for three quasars which show dramatic changes in their C iv and C iii] broad emission line properties as well as in their underlying continuum. These are some of the first examples of "Changing Look Quasars" at high ($z > 1$) redshift. Moreover, these are the first cases for substantial changes of ions with high ionization potentials (I.P.'s >2 Rydberg), thus linking the ionizing photons to the energetic inner accretion disk, potentially by inverse Compton scattering of lower energy photons to higher energies.

Details of the atomic transitions that produce strong rest-frame UV/optical lines in quasars are given in Table 1. In this paper we use the wavelengths of 1548.202 and 1550.774 Å for the C iv doublet (Kramida et al. 2018). For ionisation energies, 47.89 eV (3.519 Ry) is required for doubly-ionised C III to become triply-ionised C iv. 64.49 eV (4.74 Ry) is the energy needed to ionize C iv itself. This energy corresponds to a thermal temperature of $T \gtrsim 4{\times}10^5$, implying a heating energy source of (soft) X-ray photons.

Wilhite et al. (2006) examine C iv variability in a sample of 105 quasars observed at multiple epochs by the Sloan Digital Sky Survey (SDSS; York et al. 2000; Stoughton et al. 2002; Abazajian et al. 2009a). They find a strong correlation between the change in the C iv line flux and the change in the line width, but no correlations between the change in flux and changes in line center and skewness. These authors find that the relation between line flux change and line width change is consistent with a model in which a broad line base varies with greater amplitude than the line core. The C iv lines in these high-luminosity quasars appear to be less responsive to continuum variations than those in lower luminosity AGN.

Richards et al. (2011) explored the BEL region in over 30,000 $z > 1.54$ SDSS quasars, concentrating on the properties of the C iv emission line. These authors consider two well-known effects involving the C iv emission line: *(i)* the anti-correlation between the C iv equivalent widths (EWs) and luminosity (i.e., the Baldwin Effect; BEff) and *(ii)* the blueshifting of the peak of C iv emission with respect to the systemic redshift. We denote the velocity offset of emission lines as $V_{\rm off}$ and use the convention that a positive $V_{\rm off}$ value means the line is blueshifted while a negative $V_{\rm off}$ value means the line is redshifted. Richards et al. (2011) find the blueshift of the C iv emission line, is found to be nearly ubiquitous, with a mean shift of $V_{\rm off}$ ~810 km s^{-1} for radio-quiet (RQ) quasars and $V_{\rm off}$ ~360 km s^{-1} for radio-loud (RL) objects. Richards et al. (2011) also find the BEff is present in both the RQ and RL studied samples. These author conclude that these two C iv parameters (EQW and blueshift) are capturing an important trade-off between "disk" and "wind" components in the disk-wind model of accretion disks (e.g., Murray et al. 1995; Elvis 2000; Proga et al. 2000; Leighly 2004), with one dominating over the other depending on the shape of the SED.

Using the multi-epoch spectra of 362 quasars from the Sloan Digital Sky Survey Reverberation Mapping (SDSS-RM; Shen et al. 2015, 2019) project, Sun et al. (2018) investigate the blueshift of C iv emission relative to Mg ii emission, and its dependence on quasar properties. These authors confirm that high-blueshift sources tend to have low C iv EWs, and that the low-EW sources span a range of blueshift. Other high-ionization lines, such as [He ii] , also show similar blueshift properties. The ratio of the line width of C iv to that of Mg ii increases with blueshift. Sun et al. (2018) also find that quasar variability might slightly enhance the connection between the C iv blueshift and EW, though further investigation here is warranted. There is also the finding that the objects with that largest blueshifts are less variable and tend to have higher Eddington ratios. Sun et al. (2018) explain their results these by suggesting that quasar SEDs have weaker X-ray emission (or at least a larger UV/optical-to-Xray spectral index, $\alpha_{\rm ox}$) and thus become *softer* with *increasing Eddington ratio* along with the presence of X-ray shielding by the inner accretion disk. However, a high Eddington ratio alone might be an insufficient condition for the C iv blueshift. Recent investigations also include Meyer et al. (2019) and Doan et al. (2019). Dyer et al. (2019) provide a detailed analysis of 340 quasars at high-redshift ($1.62 < z < 3.30$) from the SDSS-RM project, which we will compare our results to.

The purpose of this paper is, for the first time, to systematically access and report on the CLQ phenomenon at high ($z > 2$) redshift. While accessing this phenomenon at an earlier cosmic epoch is somewhat interesting, the main value of this study is we move from the low-ionization energy Balmer emission line series to the high-ionization emission lines, in particular C iv λ1549.

of a *large number* of AGN and second, the *intrinsic* Baldwin effect, the same anti-correlation but in an *individual, variable* AGN (Pogge & Peterson 1992).

Object	Redshift	g-band (mag)	MJD	Instrument	Exposure Time (secs)	SDSS Plate-FiberID	Notes
	2.068	18.27	53498	SDSS	8057	2089-427	
J120544.7+342252.4	2.071		58538	DBSP	1800	—	Average conditions
	2.071		58693	DBSP	2400	—	
	2.185	19.77	54553	SDSS	4801	2948-614	
J163852.9+282707.7	2.186		55832	BOSS	3600	5201-178	
	2.182		58583	LRIS	1800	—	
	2.217	19.97	56189	BOSS	2700	6118-720	
J222818.7+220102.9	2.222		56960	BOSS	4500	7582-790	eBOSS reobservation
	2.222		58693	DBSP	2400	—	

Table 2. Details of our spectroscopic observations. Redshift errors are typically ±0.002. SDSS, BOSS and eBOSS spectra have $\mathcal{R}$ ~2,000. DBSP: Double Spectrograph on the Palomar 200-inch telescope. LRIS: Low Resolution Imaging Spectrometer on Keck I 10m telescope.

This paper is organised as follows. In Section 2, we describe our sample selection, catalogues, and observational data sets. In Section 3, we show the high-z quasars and report the line properties for the quasars at the observed epochs. We give a very brief theoretical discussion in Section 4. We present our conclusions in Section 5. We report all magnitudes on the AB zero-point system (Oke & Gunn 1983; Fukugita et al. 1996) unless otherwise stated. For the WISE bands, $m_{\rm AB} = m_{\rm Vega} + m$ where $m = (2.699, 3.339)$ for WISE W1 at 3.4μm and WISE W2 at 4.6μm, respectively (Cutri et al. 2011; Cutri 2013). We adopt a flat ΛCDM cosmology with $\Omega_\Lambda = 0.73$, $\Omega_{\rm M} = 0.27$, and $h = 0.71$. All logarithms are to the base 10.

2 DATA, CLQ SELECTION AND LINE MEASUREMENTS

In this section we present the photometric data used to select the CLQs, and then give details to the multiwavelength data where we have it. We then give details of the spectroscopic data including emission lines measurements.

2.1 Photometry

2.1.1 Optical Photometry

We use optical data from the Catalina Real-time Transient Survey (CRTS; Drake et al. 2009; Mahabal et al. 2011), the Panoramic Survey Telescope and Rapid Response System (PanSTARRS; Kaiser et al. 2010; Stubbs et al. 2010; Tonry et al. 2012; Magnier et al. 2013) and the Zwicky Transient Facility (ZTF; Bellm et al. 2019a).

The CRTS archive[2] contains the Catalina Sky Survey data streams from three telescopes – the 0.7 m Catalina Sky Survey (CSS) Schmidt and 1.5 m Mount Lemmon Survey (MLS) telescopes in Arizona and the 0.5 m Siding Springs Survey (SSS) Schmidt in Australia. CRTS covers up to ~2500 deg^2 per night, with 4 exposures per visit, separated by 10 min. The survey observes over 21 nights per lunation. The data are broadly calibrated to Johnson V (see Drake et al. 2013, for details) and the current CRTS data set contains time series for approximately 400 million sources to $V \sim 20$ above Dec > -30 from 2003 to 2016 May (observed with CSS and MLS) and 100 million sources to $V \sim 19$ in the southern sky from 2005 to 2013 (from SSS). CRTS has been used to study distant quasars previously (Graham et al. 2014, 2015a,b, 2017, 2019a).

PanSTARRS data is obtained via the Pan-STARRS Catalog Search interface[3]. We query the PS1 DR2 Detection catalog.

The ZTF is a new robotic time-domain sky survey capable of visiting the entire visible sky north of -30 deg. declination every night. ZTF observes the sky in the g, r, and i-bands at different cadences depending on the scientific program and sky region (Bellm et al. 2019b; Graham et al. 2019b). The ZTF 576 megapixel camera with a 47 deg^2 field of view, installed on the Samuel Oschin 48-inch Schmidt Telescope, can scan more than 3750 deg^2 per hour, to a 5σ detection limit of 20.7 mag in the r-band with a 30sec exposure during new moon (Masci et al. 2019).

2.2 Multi-Wavelength Properties

DS to write something on FIRST non-detections; possibly check the X-rays too?
Mid-infrared data (3.4 and 4.6μm) is available from the beginning of the *Wide-field Infrared Survey Explorer* (*WISE*) mission (2010 January; Wright et al. 2010) through the fifth-year of *NEOWISE-R* operations (2018 December; Mainzer et al. 2011). The *WISE*WISE scan pattern leads to coverage of the full-sky approximately once every six months (a "sky pass"), but the satellite was placed in hibernation in 2011 February and then reactivated in 2013 October. Hence, our light curves have a cadence of 6 months with a 32-month sampling gap.

2.3 CLQ Selection

MJG to finalise this
Our high-z CLQs were identified as follows. We selected all 64,774 SDSS DR15 sources with $z > 0.35$ classified as 'quasar', having at least two spectra separated by at least 100 days, and with a corresponding CRTS light curve. We fitted a damped random walk to the CRTS data via Gaussian process regression and the photometric magnitudes at the epochs of the SDSS spectra for a given source are predicted. Those where $|\Delta V| > 0.3$ are then selected for visual inspection. Only three quasars SDSS J120544.7+342252.4 (hereafter J1205+3422), SDSS J163852.93+282707.7 (hereafter J1638+2827) and SDSS J222818.76+220102.9 (hereafter J2228+2201), satisfied these selection criteria and showed interesting or dramatic emission line behaviour.

[2] http://catalinadata.org

[3] https://catalogs.mast.stsci.edu/panstarrs/

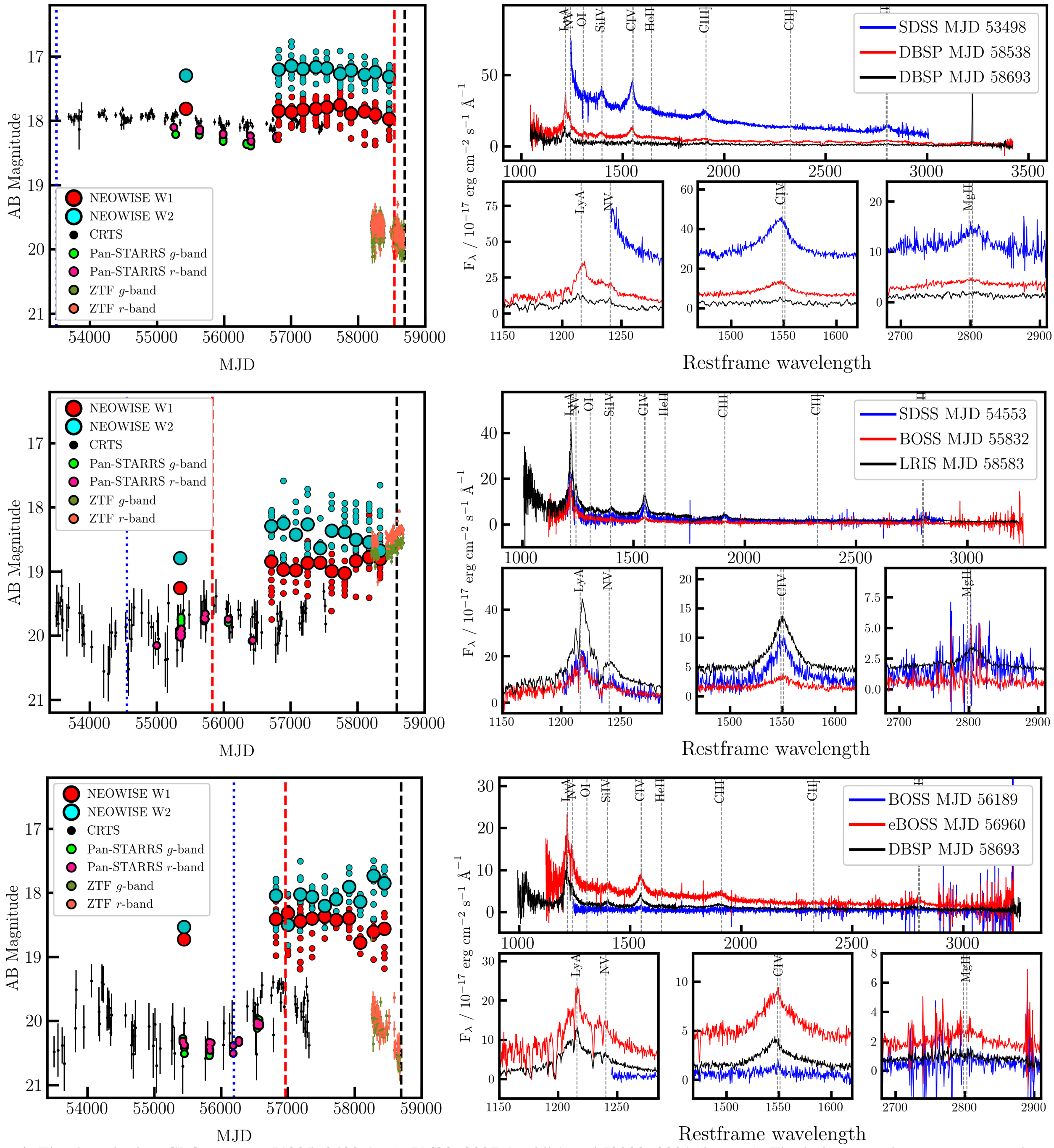

Figure 1. The three high-z CLQ quasars; J1205+3422 (top), J1638+2827 (middle) and J2228+2201 (bottom). The light curve data is present in the panels on the left hand side, with the spectral epoch observational timings indicated by vertical lines. The spectra are on the right hand side, with zoom-in's on the Lyα-N v complex, the C iv line, and the Mg ii line.

2.4 Spectroscopy

An overview of our spectroscopic observations is given in Table 2. The spectra are from the SDSS (Stoughton et al. 2002; Abazajian et al. 2009b; Schneider et al. 2010), the SDSS-III Baryon Oscillation Spectroscopic Survey (BOSS; Eisenstein et al. 2011; Dawson et al. 2013; Smee et al. 2013; Alam et al. 2015; Pâris et al. 2017) and the SDSS-IV Extended Baryon Oscillation Spectroscopic Survey (eBOSS; Dawson et al. 2016; Abolfathi et al. 2018; Pâris et al. 2018). These quasars were targetted via a range of techniques and algorithms (see Richards et al. 2002; Ross et al. 2012; Myers et al. 2015). The SDSS, BOSS, and eBOSS data are supplemented by spectra from the Low Resolution Imaging Spectrometer (LRIS; Oke et al. 1995) on the 10m Keck I telescope. and the Double Spectrograph (DBSP) instrument on the 200" Palomar telescope.

2.4.1 *Spectrophotometry*

MJG to check/finalise

We want all our spectra to have reliable flux calibrations. SDSS spectra ae spectrophotometrically calibrated. BOSS and eBOSS

Object	MJD	Cont. @ 1450Å νL_ν 10^{42} erg s^{-1}	Slope ($F_\lambda \propto \lambda^\alpha$)	CIV 1549Å Luminosity 10^{42} erg s^{-1}	FWHM km s^{-1}	V_{off} km s^{-1}	EW Å	Virial product $\log(\nu L_\nu^{0.5} \times \mathrm{FWHM}^2)$ $\log(M/M_\odot)$
J1205+3422	53498	38129 ± 39	-1.57 ± 0.01	898 ± 15	6024 ± 120	944 ± 33	37.78 ± 0.62	9.85 ± 0.02
	58538	8550 ± 11	-1.41 ± 0.01	385.2 ± 3.9	7109 ± 91	1085 ± 29	71.32 ± 0.71	9.67 ± 0.01
	58693*	2725 ± 40	-1.27 ± 0.05	161 ± 22	14997 ± 2500	922 ± 690	91.68 ± 12.73	10.07 ± 0.13
J1638+2827	54553	3579 ± 49	-1.16 ± 0.07	293.6 ± 8.8	4630 ± 180	183 ± 57	127.67 ± 3.80	9.11 ± 0.04
	55832	2340 ± 15	-2.17 ± 0.05	84.6 ± 4.2	4733 ± 290	172 ± 89	59.61 ± 2.98	9.04 ± 0.05
	58583	7793 ± 19	-2.02 ± 0.01	367.5 ± 4.3	4511 ± 71	94 ± 24	77.89 ± 0.91	9.25 ± 0.01
J2228+2201	56189*	607 ± 49	-0.00 ± 0.16	72.8 ± 11.3	14993 ± 2400	828 ± 691	162.89 ± 25.37	9.74 ± 0.14
	56960	7842 ± 25	-1.72 ± 0.02	301.0 ± 7.2	7136 ± 210	-276 ± 64	61.99 ± 1.48	9.65 ± 0.03
	58693	2388.4 ± 6.8	-1.22 ± 0.01	145.4 ± 1.5	6084 ± 83	168 ± 28	94.77 ± 0.99	9.26 ± 0.01

Table 3. Continuum at 1450Å and C IV spectral measurements for the three quasar considered in this work, at all observation epochs, as calculated by QSFit. *The C IV line is very faint (with respect to the continuum), and the associated estimates are likely unreliable. The last column shows the virial product calculated as $\nu L_\nu^{0.5} \times \mathrm{FWHM}^2$.

spectra have spectrophotometric corrections applied in the latest data release (Hutchinson et al. 2016; Jensen et al. 2016; Margala et al. 2016). Due to the high-z of our objects, [O III] is not available to us to use as a calibrating flux line. Instead we use photometric data from the ZTF since all our non-SDSS/BOSS/eBOSS data are taken after MJD 57500.

2.5 Emission Line and Power-law Slope Measurements

We use the measured quasar emission line properties from several catalogues: Shen et al. (2011), Hamann et al. (2017), Kozłowski (2017), and Calderone et al. (2017).

In particular we use the Quasar Spectral Fitting (QSFit) software package presented in Calderone et al. (2017). This provides luminosity estimates as well as width, velocity offset and equivalent width of 20 emission lines, including C IV, C III] and Mg II . We process and fit all nine spectra using the lastest version (v1.3.0) of the QSFit online calculator. The host galaxy and blended iron emission at rest-frame optical wavelengths components are automatically disabled when they can not be constrained by the available data, such as the case for all our objects (we do not have infrared spectral data). Power-law continuum slopes, α, where $f_\lambda \propto \lambda^\alpha$, are also reported in these catalogues and from QSFit. We quote the most appropriate value given the emission line wavelength.

3 RESULTS

3.1 Photometric and Overal Spectral Evolution

Figure 1 presents the optical and mid-IR light curves for three high-z CLQ quasars. Figure 1 also shows the spectra for each epoch, with the MJD of observation given by the dashed vertical lines in the light curves.

For J1205+3422, our spectral observations cover 5195 days observed, 1691 days in the rest-frame. This quasar was initially identified in SDSS in 2005 May, as a bright, $g \approx 18.0$, blue-sloped quasar with broad Si IV , C IV, C III] and Mg II . C III] and C IV have large blueshifts of ≈2600±150 and ≈1150±100 km s^{-1}, respectively. By 2019, however, the optical brightness dropped by ∼1.5 magnitudes and the spectra are significantly less blue. While Lyα and N V are detectable in both 2019 spectra, C IV has all but disappeared in the 2019 June spectrum. The broad C III] emission has disappeared between the 2005 and 2019 spectra. The changes in C IV and C III] going from broad emission to barely detectable have on the timescales of ≈50 days in the rest-frame.

For J1638+2827, our spectral observations cover 4030 days observed, 1265 days in the rest-frame. Here, in the initial epoch spectrum, C IV is broad and bright, as is C III. However, ≈400 rest-frame days later, the broad C IV and C III] BEL have faded, the continuum slope around 1400Å has changed from ≈ −1.48 to ≈ −2.25, but the Lyα /N V emission complex is very similar in shape and line flux intensity. Around 870 days in the rest-frame after the second spectral epoch, Lyα , N V , C IV, C III] and Mg II are all apparent and broad, with Mg II being seen for the first time at high signal-to-noise. The light curve is consistent with this spectral brightening, increasing from ∼20th magnitude to ∼18.5 magnitude at optical wavelengths. An absorption feature between Lyα and N V is seen in all three spectral epochs.

For J2228+2201, our spectral observations cover 2504 days observed, 778 days in the rest-frame. Over the course of 240 rest-frame days, C IV and C III] both *emerge* as BELs and the standard UV/blue continuum slope increases in flux. Then, over the course of 538 days in the rest-frame, the broadline emission, while still very present, reduces in line flux the UV/blue continuum diminishes, though is still more luminous than the initial BOSS spectrum.

3.2 C IV Emission Line Evolution

We analyzed the spectra of the three quasars, at all observational epochs, using the QSFit spectral fitting package (Calderone et al. 2017). One advantage of using QSFit is that it allows constraints on the slope and luminosity of the broad band continuum of the source. The relevant estimated quantities, including continuum luminosity and slope at rest-frame 1450Å, C IV line luminosity, FWHM and EW are given in Tabl;e 3. All fits are performed with $E(B-V) = 0$ and the best fit model in the region of the C IV emission line are shown in Figure 2.

All C IV lines are fitted with a single, broad, Lorentzian profile. This allows us to account for the narrow peak of the C IV line. No narrow components are considered for several reasons: in the epochs of highest brightness the "narrow" component would have FWHM ∼ $2-3\times10^3$ km s^{-1}, i.e. values exceeding the usual widths of genuine narrow lines ($\lesssim 10^3$ km s^{-1}); by allowing a second component, to have such large widths their parameters would become highly degenerate with the "broad" components, and the latter would also

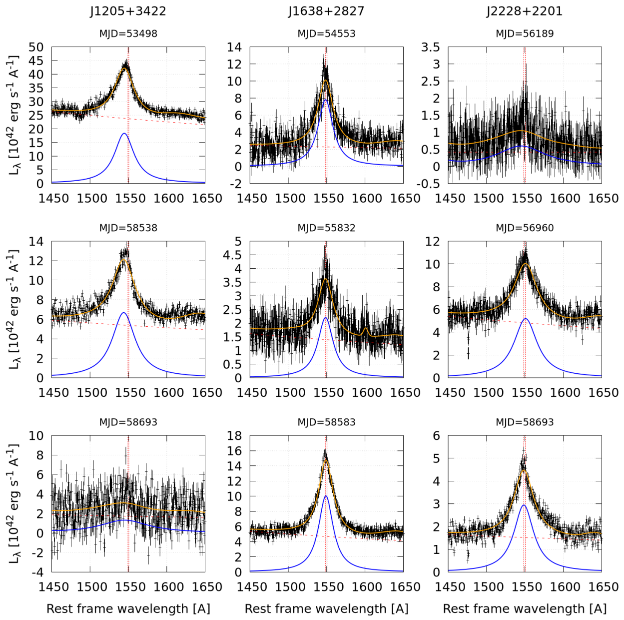

Figure 2. Observed spectra and best fit model in the region relevant to C IV emission line for the quasars considered here.

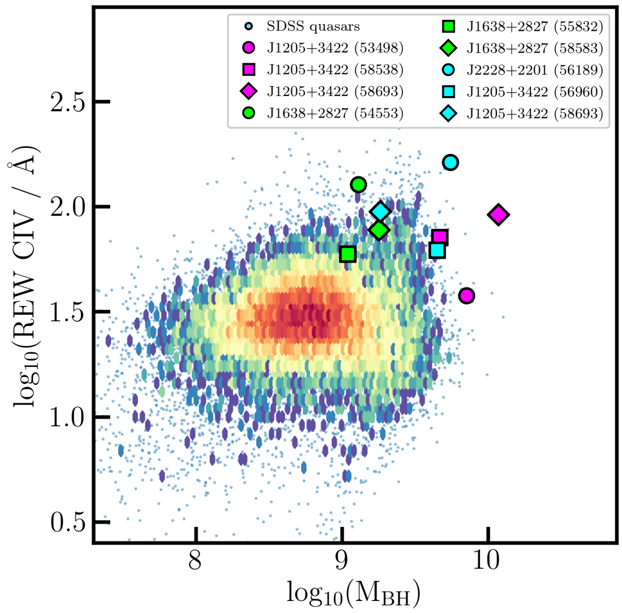

Figure 3. The virial black hole masses of ≈20,000 $z > 1.5$ quasars from QSFit catalogue (Calderone et al. 2017) and the C IV Equivalent widths. Different quasars are given different colours: J1205+3422 purple; J1638+2827 green; J2228+2201 is blue. Different epochs different symbols: first epoch circles; second epoch squares; third epoch diamonds.

have much larger FWHM (∼10^4 km s^{-1}); and by neglecting the narrow components we have a consistent fit across all epochs.

The quasar continuum, evaluated at 1450Å , and the C IV line luminosities follow a similar evolution, with a ratio of ∼20-30, confirming that the main driver for emission line variability is likely the broad band continuum itself. For all sources except J1638+2827, the slope of the continuum changes with luminosity following a "bluer-when-brighter" pattern, suggesting that a distinct emerging component is responsible or both the slope and luminosity variations. In J1638+2827 the opposite behaviour is observed, especially in the first observation epoch. However, this may be a bias due to the limited wavelength range available which extends to $\lambda \sim 1240$Å for the first epoch, while it extend to shorter wavelengths for the other epochs (respectively 1140Å and 1010Å). The latter suggests that the "emerging" component is more prominent at UV wavelengths, and a sufficient wavelength coverage is required to detect it. We find there is no need for a narrow component in J2228+2201 MJD 56189. This is because the data resemble a P-Cygni profile, with blueshifted absorption. This feature is very narrow, and the uncertainties large, such that the overall χ^2 is only marginally affected by the addition of a further component. We therefore avoid using a narrow component for this spectrum only, since that would be inconsistent with the other analyses. In all cases where the C IV line profile is reliably constrained the C IV FWHM is approximately constant, with maximum variations $\lesssim$ 1000 km s^{-1}, despite the significantly larger variations in the line luminosities.

3.3 Virial Black Hole Masses

The FWHM of broad lines is likely related to the mass of the supermassive black hole powering the quasar phenomenon, which is assumed to be constant on any human timescale. Hence it is instructive to check whether the virial product, which is the basic quantity used to calculate the single epoch black hole mass estimate, show any variation.

Using the estimates for the continuum luminosity and FWHW from the single-epoch spectra, one can estimate the central black hole mass (e.g. Shen et al. 2011; Calderone et al. 2017). This approach assumes that the broad-line region (BLR) is virialized, the continuum luminosity is used as a proxy for the BLR radius, and the broad line width (FWHM) is used as a proxy for the virial velocity. This "virial mass" estimate can then be expressed as:

$$\log(M_{\rm BH}) = (\nu L_\nu)^\gamma \times (\mathrm{FWHM})^\delta \quad (1)$$

where $\gamma = 0.5$ and $\delta = 2$. The virial product for the C IV CLQs is reported in the last column of Tab. 3. The uncertainty typically associated to the single epoch mass estimate is ∼0.5 dex, hence the virial product at all epochs are remarkably constant and compatible with a single value of black hole mass for each source, even in those cases where the C IV estimates are possibly unreliable. The object showing larger variation is J2228+2201, although the extreme values span a range of 0.48 dex.

From the virial mass estimates, all our objects have SMBH masses $M > 10^9 M_\odot$. This is at the upper end of SMBH masses at all epochs, and towards the extreme of the mass distribution for $z \sim 2$ objects. Figure 3 shows the C IV Equivalent width and the virial black hole masses for a sample of ≈20,000 $z > 1.5$ SDSS quasars from the QSFit catalog as well as the estimates for the three C IV CLQs.

3.4 Quantified Temporal Evolution of C IV Emission

Figure 4 shows the rest Equivalent Width (REW) versus the Full Width Half Maximum (FWHM) of the C IV emission line in the BOSS DR12 quasar sample using the catalogue of Hamann et al. (2017).

The velocity offsets of the C IV line are also approximately constant, and compatible with a single value (within 3σ). The exception is J2228+2201, where a significant change (∼7σ) is observed between the second and third observation epochs.

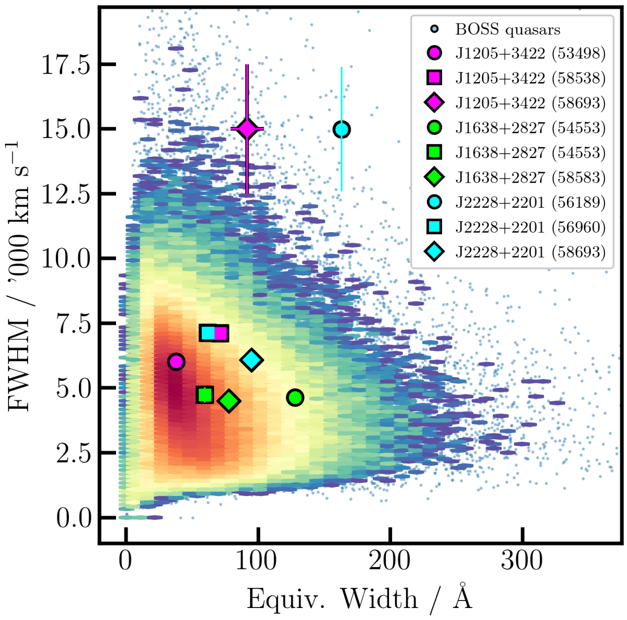

Figure 4. The Rest Equivalent Width (REW) vs. Full Width Half Maximum (FWHM) of the C IV emission line in the BOSS DR12 quasar sample using the catalogue of Hamann et al. (2017). Symbols as in Fig. 3.

The temporal evolution of the velocity offsets, along with the 1450Å continuum luminosity and slope, the C IV line FWHM and virial black hole mass are given in Figure 5.

3.5 The C IV Baldwin Effect

The Baldwin Effect (Beff; Baldwin 1977) is an empirical relation between emission-line REWs and continuum luminosity in quasars (Shields 2007; Hamann et al. 2017; Calderone et al. 2017). Hamann et al. (2017) and Calderone et al. (2017) present recent measurements of the Beff for large quasar samples.

There is an anti-correlation between the emission-line REWs and e.g. 1450Å rest continuum luminosity, so that as the underlying UV continuum luminosity increases, the EW decreses. Figure 6 shows this for a sample (from the QSFit catalogue) for 20,374 quasars. The slope (not shown) is β is −0.1997. This is consistent with Kozłowski (2017), using their bolometric luminosity gives a slope of $\beta = -0.251$ and in line with that from Hamann et al. (2017, $\beta = -0.23$).

We add the measurements from the three C IV CLQ quasars at each epoch to Figure 6. We see first that all three quasars at all three epochs lie on the edge of the νL_ν-EW distribution. Second, with the exception of J1638+2827 on MJD 55832, all the measurements show an *intrinsic Baldwin Effect* (e.g. Goad et al. 2004; Rakić et al. 2017). The slope of the CLQs intrinsic BEff is ≈ −0.38, as shown by the dashed red line in Fig. 6.

4 DISCUSSION

4.1 Continuum and Line Changes: Comparisons to recent Observations

The top row of Figure 5 demonstrates that both the 1450Å continuum and the C IV emission lines can exhibit large, >×10, changes in luminosity, *and* that these continuum-line changes track each other.

Trakhtenbrot et al. (2019) report on the quasar 1ES 1927+654 which was initially seenn to lack broad emission lines and line-of-sight obscuration, i.e, a "Type 2" quasar at redshift $z = 0.02$. This object is then seen to spectroscopically change with the appearance of a blue, featureless continuum, followed by the emergence of broad Balmer emission lines. i.e. this quasar changes into a broad-line Type 1 after a raise in the continuum luminosity. This suggests that there is (at least in some cases) a direct relationship between the continuum and broad emission lines in CLQs. A similar scenario may have occured for the 3 high-z quasars presented here, although we lack the high-cadence multiwavelength, multi-epoch coverage that Trakhtenbrot et al. (2019) present. The multiwavelength data that Trakhtenbrot et al. (2019) have includes a UV spectrum of 1ES 1927+654. Interestingly, however, there is no evidence for broad UV emission lines, including C IV, C III, or Mg II. The authors attribute the lack of broad UV emission lines to dust within the BLR, noting that to dust in the broadline emission region, noting that the continuum emission does not show any signs of dust extinction.

MacLeod et al. (2019) present a sample of CLQs where the primary selection requires large-amplitude ($|\Delta g| > 1$ mag, $|\Delta r| > 0.5$ mag) variability over any of the available time baselines probed by the SDSS and Pan-STARRS1 surveys. They find 17 new CLQs which is ∼20% of the observerd sample. This CLQ fraction increases from 10% to roughly half, as the continuum flux ratio between repeat spectra at 3420 Å (rest-frame) increases from 1.5 to 6. MacLeod et al. (2019) note that these candidates are at lower Eddington ratio relative to the overall quasar population.

Using the same dataset as and extremely variable quasar sample as MacLeod et al. (2019), Homan et al. (2019) investigate the responsiveness of the Mg II broad emission line doublet in AGN on timescales of several years. By again focussing on quasars that show large changes in their optical light-curves, Homan et al. (2019) find that Mg II clearly does respond to the continuum. However, a key finding from Homan et al. (2019) is that the degree of responsivity varies strikingly from one object to another. There are cases of Mg II changing by as much as the continuum, more than the continuum, or very little at all. In the majority (72%) of this highly variable sample, the behaviour of Mg II corresponds with that of Hβ. However, there are also examples of Mg II showing variation, but Hβ does not, and vice versa.

4.2 Continuum and Line Changes: Comparisons to theoretical expectaions

SF and BM to add a little more here

The C IV line is one of the strongest collisionally excited lines in quasar spectra (e.g. Hamann & Ferland 1999), and C IV emission probes the photoionization environment produced by the innermost disk, as indicated by RM time-delay measurements.

In standard Shakura & Sunyaev (1973) thin disk models, large changes in the continuum flux are not permitted over short timescales due to the relatively long viscous time associated with such disks. Given the observed short timescale continuum variations, it is not surprising that the Shakura & Sunyaev (1973) disk may fail on other fronts.

This indicates they may comfortably fit into the sample of C IV variable quasars explored by Dyer et al. (2019), and similar to those authors we suggest slim accretion disk models e.g., Abramowicz et al. (1988) or inhomogeneous disk models (e.g., Dexter & Agol 2011) may provide viable explanations for our observations.

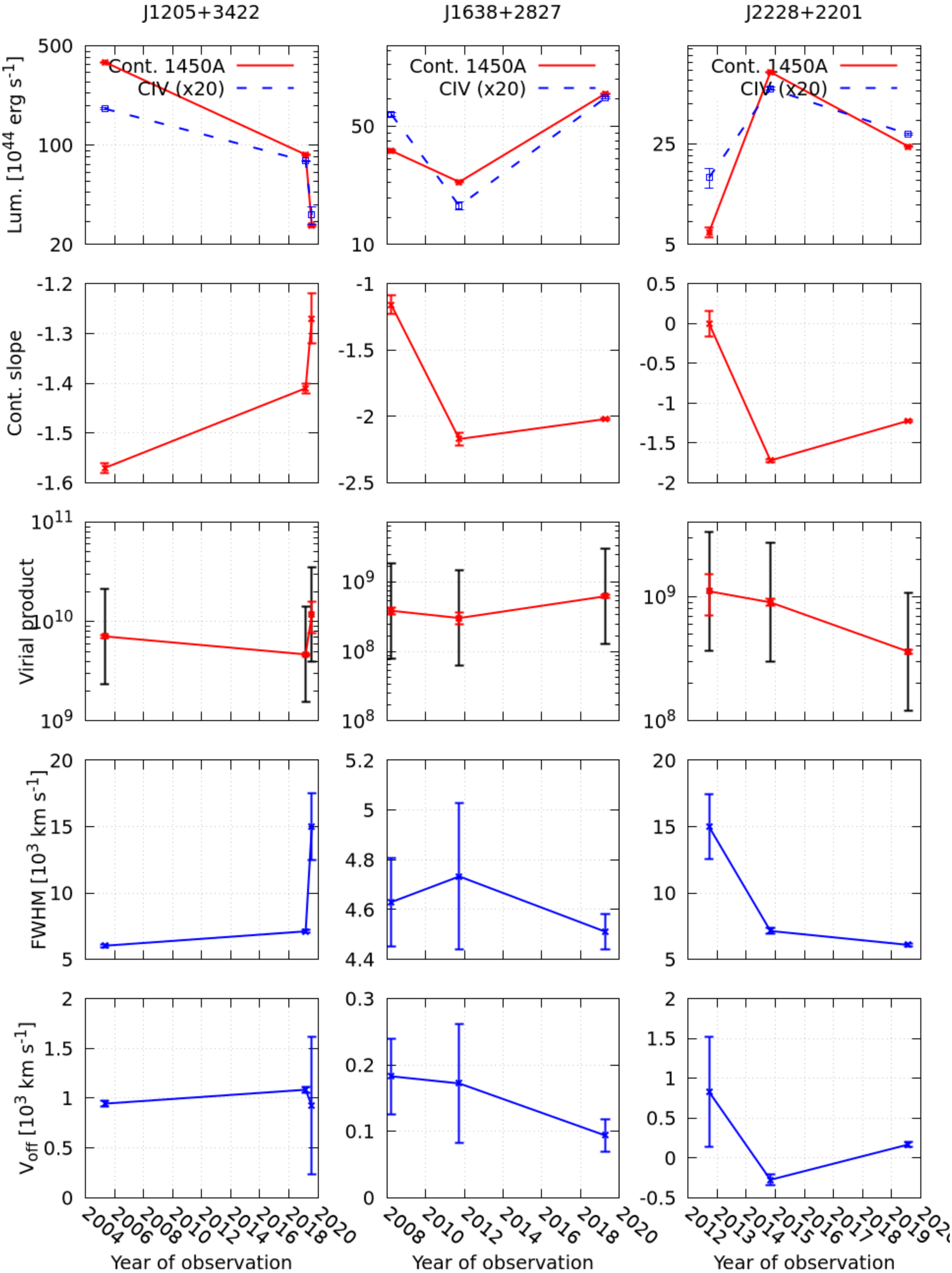

Figure 5. Temporal evolution of the spectral properties of the three quasar considered in this work.

Object	MJD	M_i	$L_{\rm bol}$	$M_{\rm BH}$ Mg II	$M_{\rm BH}$ C IV	$\eta_{\rm Edd}$ Mg II	$\eta_{\rm Edd}$ C IV	Ref.
J1205+3422	53498	-27.74	47.216±0.004	9.55±0.05	9.49±0.04	-0.434	-0.374	Shen11
	58538							
	58693							
J1638+2827	54553	-26.75	46.166±0.04	9.03±0.37	8.74±0.15	-0.964	-0.677	Shen11
	55832	-26.40	46.721±0.073	9.34	9.13	-0.717	-0.509	Kozl17
	58583							
J2228+2201	56189	-25.46	46.231±0.073	9.45	8.73	-1.317	-0.602	Kozl17
	56960							
	58693							

Table 4. Physical properties of the C IV CLQs. $M_{\rm I}(z=2)$ is the Absolute i-band magnitude K-corrected to $z=2$; Bolometric luminosity computed from the monochromatic luminosity at 1350Å using the spectral fits and bolometric corrections (BC = 3.81) in Richards et al. (2006). Virial BH masses using calibrations of Vestergaard & Peterson (2006). $\eta_{\rm Edd}$ is the base 10 logarithm of the Eddington ratio computed using the virial BH mass. Shen11 is Shen et al. (2011). Kozl17 is Kozłowski (2017).

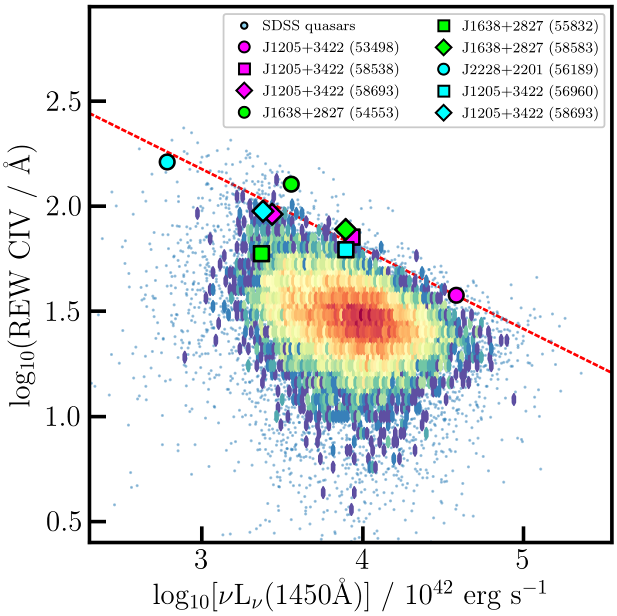

Figure 6. The C IV Equivalent width and the underlying continuum luminosity, commonly referred to as The Baldwin Plot. The continuum luminosities are from Calderone et al. (2017), the REW measurements are Table 3. Symbols as in Fig. 3. The dashed red line has slope $\beta = -0.38$.

4.3 Implications for The Baldwin Effect

The variable properties of the rest-frame UV quasar emission lines have been long studied, with the global (or ensemble) Baldwin Effect (the anti-correlation between the EW of the emission line and the underlying continuum luminosity of single-epoch observations of a large number of AGN, first noted in Baldwin (1977). More recently, the intrinsic Baldwin effect, the same anti-correlation but in an individual, variable AGN.

The X-ray Baldwin Effect (e.g., Iwasawa & Taniguchi 1993)... Bachev et al. (2004) find a 10-fold decrease in EW C IV with Eddington ratio (decreasing from ~1 to ~0.01), while N V shows no change. These trends suggest a luminosity-independent "Baldwin effect" in which the physical driver may be the Eddington ratio. Ge et al. (2016) Broad emission lines is a prominent property of Type 1 quasars.

4.4 Eddington Ratios and State Changes

The broad UV and optical lines in quasars are most sensitive to the extreme ultraviolet (EUV) part of the spectral energy distribution (SED), with C IV (and indeed [He II] and N V) being at the higher energy end of the EUV distribution.

The soft X-ray excess – the excess of X-rays below 2 keV with respect to the extrapolation of the hard X-ray spectral continuum model – is a very common feature among type 1 active galactic nuclei (AGN). Noda & Done (2018) note that The soft X-ray excess produces most of the ionizing photons, so its dramatic drop leads to the disappearance of the broad-line region, driving the "changing-look" phenomena. major difference is that radiation pressure should be much more important in AGNs, so that the sound speed is much faster than expected from the gas temperature. This spectral hardening appears similar to the soft-to-hard state transition in black hole binaries at $L/L_{\rm Edd} \sim 0.02$ (i.e. $\eta_{\rm Edd} \sim -1.7$), where the inner disc evaporates into an advection dominated accretion flow, while the overall drop in luminosity appears consistent with the hydrogen ionization disc instability. Crucially Noda & Done (2018) make the prediction that all changing-look AGNs are similarly associated with the state transition at $L/L_{\rm Edd}$ ~a few per cent.

By comparing the observed correlations between the UV/optical-to-X-ray spectral index ($\alpha_{\rm ox}$) and Eddington ratio in AGN to those predicted from observations of X-ray binary outbursts, Ruan et al. (2019) find a remarkable similarity to accretion state transitions in prototypical X-ray binary outbursts, including an inversion of this correlation at a critical Eddington ratio of $\sim 10^{-2}$ (i.e. at the same ratio as motivated by Noda & Done (2018)). These results suggest that the structures of black hole accretion flows directly scale across a factor of $\sim 10^8$ in black hole mass and across different accretion states. Using Ruan et al. (2019) as a guide, there are potentially three accretion regimes: (1) a "High/Soft State" with $\eta_{\rm Edd} \gtrsim -1$; (1) a "Low/Hard State" with $-2 \lesssim \eta_{\rm Edd} \lesssim -1$; (1) a "High/Soft State" with $\eta_{\rm Edd} \lesssim -2$. These are given as shaded regions in Figure 7.

Building on a previous work (e.g., Jiang et al. 2014, 2016, 2019b), Jiang et al. (2019a) use global three dimensional radiation magneto-hydrodynamic simulations to study the properties of inner regions of accretion disks around a 5×10^8 M$_\odot$ black hole with mass accretion rates reaching 7% and 20% of the Eddington value.

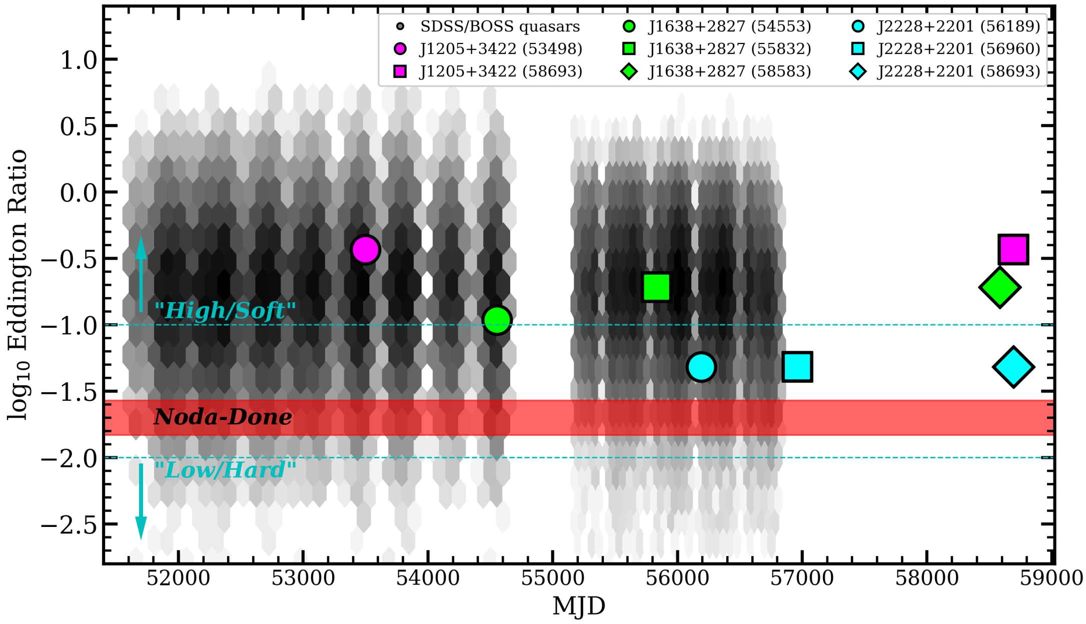

Figure 7. Eddington Ratios of the three C IV CLQs and M87.

5 CONCLUSIONS

In this paper we have reported on three redshift $z > 2$ quasars with dramatic changes in their C IV emission lines, the first 'Changing-Look" quasars at high redshift. This is also the first time the changing-look behaviour has been seen in a high-ionization emission line.

- SDSS J1205+3422, J1638+2827 and J2228+2201 show interesting behaviour in their observed optical light curves, and subsequent spectroscopy shows significant changes in the C IV broad emission line, with both line collapse and emergence being displayed in rest-frame timescales of ∼240-1640 days.
- Where observed, the profile of the Lyα/N V emission complex also changes, and there is tentative evidence for changes in the Mg II line.
- Although line measurements from the three quasars show large changes in the C IV line flux-line width plane, the quasars are not seen to be outliers when considered against the full $z > 2$ quasar population in terms of (rest) Equivalent Width and FWHM properties.
- We put these observations in context with recent "state-change" models, but note that even in their 'low-state', the C IV CLQs are above ∼ 10% in Eddington luminosity.

Availability of Data and computer analysis codes

All materials, databases, data tables and code are fully available at: https://github.com/d80b2t/CIV_CLQs.

ACKNOWLEDGEMENTS

NPR acknowledges support from the STFC and the Ernest Rutherford Fellowship scheme.

We thank:

∘ Andy Lawrence, Mike Hawkins and David Homan for useful discussion.

This paper heavily used TOPCAT (v4.4) (Taylor 2005, 2011). This research made use of Astropy, a community-developed core Python package for Astronomy (Astropy Collaboration et al. 2013; The Astropy Collaboration et al. 2018).

Funding for SDSS-III has been provided by the Alfred P. Sloan Foundation, the Participating Institutions, the National Science Foundation, and the U.S. Department of Energy Office of Science. The SDSS-III web site is http://www.sdss3.org/. SDSS-III is managed by the Astrophysical Research Consortium for the Participating Institutions of the SDSS-III Collaboration including the University of Arizona, the Brazilian Participation Group, Brookhaven National Laboratory, Carnegie Mellon University, University of Florida, the French Participation Group, the German Participation Group, Harvard University, the Instituto de Astrofisica de Canarias, the Michigan State/Notre Dame/JINA Participation Group, Johns Hopkins University, Lawrence Berkeley National Laboratory, Max Planck Institute for Astrophysics, Max Planck Institute for Extraterrestrial Physics, New Mexico State University, New York University, Ohio State University, Pennsylvania State University, University of Portsmouth, Princeton University, the Spanish Participation Group, University of Tokyo, University of Utah, Vanderbilt University, University of Virginia, University of Washington, and Yale University.

This publication makes use of data products from the Wide-field Infrared Survey Explorer, which is a joint project of the University of California, Los Angeles, and the Jet Propulsion Laboratory/California Institute of Technology, and NEOWISE, which is a project of the Jet Propulsion Laboratory/California Institute of Technology. WISE and NEOWISE are funded by the National Aeronautics and Space Administration. No animals were harmed in the production of this paper, but there was a large spider in NPRs apartment that "vanished".

REFERENCES

Abazajian K. N., et al., 2009a, ApJS, 182, 543
Abazajian K. N., et al., 2009b, ApJS, 182, 543
Abolfathi et al., 2018, ApJS, 235, 42
Abramowicz M. A., Czerny B., Lasota J. P., Szuszkiewicz E., 1988, ApJ, 332, 646
Alam S., et al., 2015, ApJS, 219, 12
Alloin D., Pelat D., Phillips M., Whittle M., 1985, ApJ, 288, 205
Antonucci R., 2018, Nature Astronomy, 2, 504
Astropy Collaboration et al., 2013, Astron. & Astrophys., 558, A33
Bachev R., Marziani P., Sulentic J. W., Zamanov R., Calvani M., Dultzin-Hacyan D., 2004, ApJ, 617, 171
Baldwin J. A., 1977, ApJ, 214, 679
Bellm E. C., et al., 2019a, PASP, 131, 018002
Bellm E. C., et al., 2019b, PASP, 131, 068003
Bian W.-H., Fang L.-L., Huang K.-L., Wang J.-M., 2012, MNRAS, 427, 2881
Calderone G., et al., 2017, MNRAS, 472, 4051
Cutri R. M. o., 2013, Technical report, Explanatory Supplement to the AllWISE Data Release Products. IPAC/Caltech
Cutri R. M., et al., 2011, Technical report, Explanatory Supplement to the WISE Preliminary Data Release Products. IPAC/Caltech
Dawson K., et al., 2013, AJ, 145, 10
Dawson K. S., Kneib J.-P., et al., 2016, AJ, 151, 44
Dexter J., Agol E., 2011, ApJ Lett., 727, L24
Doan A. N., et al., 2019, in American Astronomical Society Meeting Abstracts #233. p. 242.23
Drake A. J., et al., 2009, ApJ, 696, 870
Drake A. J., et al., 2013, ApJ, 763, 32
Dyer J. C., Dawson K. S., du Mas des Bourboux H., Vivek M., Bizyaev D., Oravetz A., Pan K., Schneider D. P., 2019, ApJ, 880, 78
Eisenstein D. J., Weinberg D. H., et al., 2011, AJ, 142, 72
Elvis M., 2000, ApJ, 545, 63
Fukugita M., Ichikawa T., Gunn J. E., Doi M., Shimasaku K., Schneider D. P., 1996, AJ, 111, 1748
Ge X., Bian W.-H., Jiang X.-L., Liu W.-S., Wang X.-F., 2016, MNRAS, 462, 966
Goad M. R., Korista K. T., Knigge C., 2004, MNRAS, 352, 277
Graham M. J., Djorgovski S. G., Drake A. J., Mahabal A. A., Chang M., Stern D., Donalek C., Glikman E., 2014, MNRAS, 439, 703
Graham M. J., et al., 2015a, MNRAS, 453, 1562
Graham M. J., et al., 2015b, Nat, 518, 74
Graham M. J., Djorgovski S. G., Drake A. J., Stern D., Mahabal A. A., Glikman E., Larson S., Christensen E., 2017, MNRAS, 470, 4112
Graham M. J., et al., 2019a, arXiv e-prints, p. arXiv:1905.02262
Graham M. J., et al., 2019b, PASP, 131, 078001
Guo H., Sun M., Liu X., Wang T., Kong M., Wang S., Sheng Z., He Z., 2019, ApJ Lett., 883, L44
Hamann F., Ferland G., 1999, ARA&A, 37, 487
Hamann F., et al., 2017, MNRAS, 464, 3431
Hemler Z. S., et al., 2019, ApJ, 872, 21
Homan D., Macleod C. L., Lawrence A., Ross N. P., Bruce A., 2019, arXiv e-prints, p. arXiv:1910.11364
Hutchinson T. A., et al., 2016, AJ, 152, 205
Iwasawa K., Taniguchi Y., 1993, ApJ Lett., 413, L15
Jensen T. W., et al., 2016, ApJ, 833, 199
Jiang Y.-F., Stone J. M., Davis S. W., 2014, ApJ, 796, 106
Jiang Y.-F., Davis S. W., Stone J. M., 2016, ApJ, 827, 10
Jiang Y.-F., Blaes O., Stone J., Davis S. W., 2019a, arXiv e-prints, p. arXiv:1904.01674v1
Jiang Y.-F., Stone J. M., Davis S. W., 2019b, ApJ, 880, 67
Kaiser N., et al., 2010, in Society of Photo-Optical Instrumentation Engineers (SPIE). p. 0, doi:10.1117/12.859188
Kozłowski S., 2017, ApJS, 228, 9
Kramida A., Ralchenko Y., Reader J., NIST ASD Team 2018, doi:10.18434/T4W30F,
Kramida A., Yu. Ralchenko Reader J., and NIST ASD Team 2019, NIST Atomic Spectra Database (ver. 5.7.1), [Online]. Available: `https://physics.nist.gov/asd` [2019, November 7]. National Institute of Standards and Technology, Gaithersburg, MD.
LaMassa S. M., et al., 2015, ApJ, 800, 144
Lawrence A., 2018, Nature Astronomy, 2, 102
Leighly K. M., 2004, ApJ, 611, 125
MacLeod C. L., et al., 2012, ApJ, 753, 106
MacLeod C. L., et al., 2019, ApJ, 874, 8
Magnier E. A., et al., 2013, ApJS, 205, 20
Mahabal A. A., et al., 2011, Bulletin of the Astronomical Society of India, 39, 387
Mainzer A., et al., 2011, ApJ, 731, 53
Margala D., Kirkby D., Dawson K., Bailey S., Blanton M., Schneider D. P., 2016, ApJ, 831, 157
Masci F. J., et al., 2019, PASP, 131, 018003
Matthews T. A., Sandage A. R., 1963, ApJ, 138, 30
Meyer R. A., Bosman S. E. I., Ellis R. S., 2019, MNRAS, 487, 3305
Murray N., Chiang J., Grossman S. A., Voit G. M., 1995, ApJ, 451, 498
Myers A. D., et al., 2015, ApJS, 221, 27
Noda H., Done C., 2018, MNRAS, 480, 3898
Oke J. B., Gunn J. E., 1983, ApJ, 266, 713
Oke J. B., et al., 1995, PASP, 107, 375
Pâris I., Petitjean P., Ross N. P., et al., 2017, Astron. & Astrophys., 597, A79
Pâris I., et al., 2018, Astron. & Astrophys.
Pogge R. W., Peterson B. M., 1992, AJ, 103, 1084
Proga D., Stone J. M., Kallman T. R., 2000, ApJ, 543, 686
Rakić N., La Mura G., Ilić D., Shapovalova A. I., Kollatschny W., Rafanelli P., Popović L. Č., 2017, Astron. & Astrophys., 603, A49
Richards G. T., et al., 2002, AJ, 123, 2945
Richards G. T., et al., 2006, ApJS, 166, 470
Richards G. T., et al., 2011, AJ, 141, 167
Ross N. P., et al., 2012, ApJS, 199, 3
Ross N. P., et al., 2018, MNRAS, 480, 4468
Ruan J. J., Anderson S. F., Eracleous M., Green P. J., Haggard D., MacLeod C. L., Runnoe J. C., Sobolewska M. A., 2019, arXiv e-prints, p. arXiv:1903.02553v1
Schneider D. P., et al., 2010, AJ, 139, 2360
Shakura N. I., Sunyaev R. A., 1973, Astron. & Astrophys., 24, 337
Shen Y., et al., 2011, ApJS, 194, 45
Shen Y., et al., 2015, ApJS, 216, 4
Shen Y., et al., 2019, ApJS, 241, 34
Shields J. C., 2007, in Ho L. C., Wang J. W., eds, Astronomical Society of the Pacific Conference Series Vol. 373, The Central Engine of Active Galactic Nuclei. p. 355 (`arXiv:astro-ph/0612613`)
Smee S. A., et al., 2013, AJ, 146, 32
Stern D., et al., 2018, ApJ, submitted
Stoughton C., et al., 2002, AJ, 123, 485
Stubbs C. W., et al., 2010, ApJS, 191, 376
Sun M., Xue Y., Richards G. T., Trump J. R., Shen Y., Brandt W. N., Schneider D. P., 2018, ApJ, 854, 128
Taylor M. B., 2005, in Shopbell P., Britton M., Ebert R., eds, Astronomical Society of the Pacific Conference Series Vol. 347, Astronomical Data Analysis Software and Systems XIV. p. 29
Taylor M., 2011, TOPCAT: Tool for OPerations on Catalogues And Tables, Astrophysics Source Code Library (ascl:1101.010)
The Astropy Collaboration et al., 2018, preprint, (`arXiv:1801.02634v2`)
Tonry J. L., et al., 2012, ApJ, 750, 99
Trakhtenbrot B., et al., 2019, ApJ, 883, 94
Vestergaard M., Peterson B. M., 2006, ApJ, 641, 689
Wilhite B. C., Vanden Berk D. E., Brunner R. J., Brinkmann J. V., 2006, ApJ, 641, 78
Wright E. L., et al., 2010, AJ, 140, 1868
York D. G., et al., 2000, AJ, 120, 1579

This paper has been typeset from a TEX/LATEX file prepared by the author.